Wake flow past an ALUTEC profile

Daniel Duda[1,*], *Yasar* Dokak[1], *Vitalii* Yanovych[1], and *Václav* Uruba[1,2]

[1]Faculty of Mechanical Engineering, University of West Bohemia, Pilsen, Czech Republic
[2]Institute of Thermomechanics, Czech Academy of Sciences, Prague, Czech Republic

Abstract. Aluminum construction profiles become a standard construction material for short-term stands in science and in industry as well. It has the shape of square prism with an groove in each side to easy connecting the nut or bolt in any location. We studied the wake past the profile of 45 mm side. We studied the topology of the wake in the dependence on the angle of attack by using the Particle Image Velocimetry technique.

1 Introduction

Due to its properties and the development of mechanical, thermal and chemical processing technologies, the aluminum profile is increasingly used in various fields: in the aircraft industry, shipbuilding, car building, in the construction of subways, in the electronic industry, in the food industry, in mechanical engineering, in the automotive industry, in the electrical industry and instrument making, household appliances, etc.

Aluminum alloys possess a number of advantages, and that led to their wide application in various industries. In particular, this high mechanical strength at low density, resistance to weathering, durability, significant compared with competing materials, turnaround time, good machinability pressure and cutting, flexibility, high cold resistance, the possibility of recycling with little energy consumption etc.

Aluminum systems offer almost unlimited possibilities for architectural design of buildings and structures. In addition, the use of this metal in architecture and construction is advantageous in the process of operation, and due to its exceptional corrosion resistance, aluminum is valued as one of the most convenient raw materials for recycling. The wide use aluminum due to its high strength, durability and workability.

It is these characteristics that determine the broad prospects for the development of the use of aluminum profiles for 15-20 years in advance. The market for the consumption of aluminum and aluminum alloy profiles is currently one of the fastest growing in the world.

The raw materials for the production of profiles are technical aluminum and wrought aluminum alloys obtained by alloying primary aluminum or aluminum scrap with alloying additives. ALUTEC KK Structural Aluminum System (ALS) was introduced to the market 25 years ago, and currently includes more than 100 versions of aluminum profiles and more than 1500 a ccessories. A key component of the entire structural system is an aluminum profile with a longitudinal track.

The structural aluminum system offers an operational and functional solution for various industries. It is characterized by simplicity and speed of installation, as well as high adaptability to other structural systems. Any part of it can be connected to the rest without the use of special tools or the need for a strong (one-piece) connection, which is welding.

The aluminum constructional system allows the production of frames, single-purpose or serial machines, ensuring the safety of workstations and machines, workbenches, trolleys, transport systems, assembly lines, conveyors, manipulators and entire workstations from standard parts. The system can be used in industrial premises, provided compatibility with ESD. The profiles are made of Al Mg Si 0.5 F 25 material in accordance with DIN 3.3206.72, and processed by natural eloxification (thickness 15 μm). This type of surface treatment improves the functional properties of the base alloy, increases the corrosion resistance, hardness and wear resistance of the profile [1].

The advantages of the ALUTEC KK system are as follows: dismantling (reconfiguration), reuse of system elements; low system weight (1/3 of the weight compared to steel); high accuracy, durability and service life of parts; simplicity, fast and intuitive work with elements; application does not require expensive equipment; application in interiors and exteriors; adaptability to other solutions and new requirements.

2 Experimental setup

2.1 Wind tunnel

We used a new wind tunnel developed by the company WTtech. The radial compressor power is controlled automatically to keep a constant velocity, which is measured as

*e-mail: dudad@kke.zcu.cz

a pressure drop on a confuser just before the test-section. The projected maximum wind speed is 90 m/s, but it still a subject of testing and optimization.

2.2 The obstacle and its position

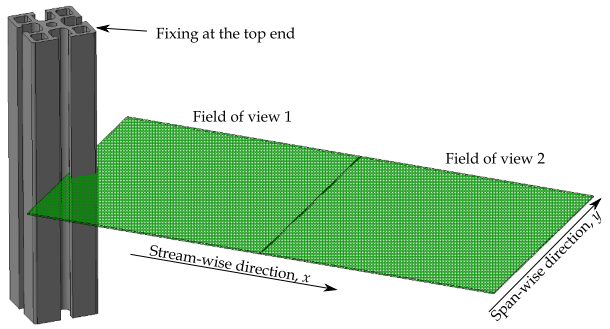

Fig. 1. Sketch of the positions of both fields of view relative to the obstacle. Obstacle dimensions: $45 \times 45 \times 200$ mm, field of view dimensions: 164×164 mm, distance of FoVs from the axis of the obstacle: 17 mm and 180 mm.

The aerodynamic tunnel at which the study was conducted has a closed test section. The height and width of this camera are 305×203 mm respectively, and the length of the test section is 745 mm. The side walls and bottom of the test section are made in the form of a monoblock of extruded polycarbonate. Characterized by high optical purity. Whereas the upper wall is modular and allows to combine its parts according to the necessity of the experiment.

The ALUTEK KK profile, measuring 45×45 mm in length and 200 mm in length, was used for the experimental studies. A through mounting hole was used to mount this profile in the middle of the test section. In which the threaded connection M8 was made. A similar hole was made in the modular section to cover the test section. Then test specimen and part of the coating section were fastened by the M8 screw. This type of connection is convenient. Because when you change the angle of the profile in the middle of the section, you only need to turn the screw with the profile to a given angle. It should also be noted that as a result of mounting the profile, there is a remained a distance of 3 mm between the profile and the bottom of the test section in order to avoid damaging the bottom desk.

2.3 Particle Image Velocimetry technique

Particle Image Velocimetry technique (PIV) [2] is in its principle a very simple method: it is based on observing the motion of small particles carried by a transparent fluid. Then we use the assumption, that small particles follow the motion of the fluid as the viscous drag dominates their own inertia, buoyancy and other hydrodynamical forces connected with local flow accelerations. In this measurement, we used droplets of oil-glycerol solution as a tracer particles. This fog produced by commercially available fog generator Safex and the particle size is in order of microns. The use of this „theater fog“ has been proven by the world-wide experience e.g. in [3–5] and many others.

These particles are illuminated in one plane of small thickness less than 1 mm. This plane of light is in our case produced by a laser beam defocused in one direction by using a cylindrical diverging lens. We use the solid state laser New Wave Solo of dominant wave-length 532 nm with pulse energy up to 500 mJ. The duration of a single pulse is 5 ns. In fact, there are two lasers in single box in order to produce a *pair* of laser shots, whose interval is dependent on velocity and we used 200 μs for the velocity mainly discussed in this article 5 m/s.

The illuminated particles are observed by using a camera and the figure is processed in computer by using an appropriate software. In the current measurement we used CCD camera MkII with spatial resolution 2048 pixels. This camera is able to distinguish both frames illuminated by the two laser shots. The objectives focus length 60 mm lead to the resolution of the grid of the velocity vectors of 2.6 mm at size of 32 pixels. We used the Dantec Dynamic Studio software for data analysis.

3 Observation

3.1 Averaged fields

The time-averaged data shows the pair of recirculation bubbles in the near-wake region as visible in the spatial distribution of the span-wise velocity shown in figure 2.

The back flow in the near-wake region is visible also in the stream-wise profile of the average stream-wise velocity displayed in figure 3 as a region with stream-wise velocity smaller than zero.

The fact, that the angle of attack changes, causes different crosssectional size of the obstacle: at $\alpha = 0°$, i.e. when the sides are perpendicular to the incoming flow, its crosssectional size is just the side of the profile, i.e. $a = 45$ mm, at $\alpha = 45°$, the crosssectional size is $\sqrt{2} \cdot a = 63.6$ mm. This change can have stronger effect on the values of turbulent kinetic energy (displayed in figure 4) and on the recovery of the stream-wise velocity in the wake (displayed in figure 3bottom), and to the position of saddle point in the wake.

Similarly, we can discuss, if the definition of Reynolds number is correct, when it is based on the side of the obstacle, not on the crosssectional size. In that case, the imposed velocity should change in order to keep the Reynolds number constant. In the present study we keep the standards used in the literature and we use the size of obstacle side as the characteristic dimension in the Reynolds number definition, which causes, that the constant imposed velocity signifies constant Reynolds number. Physically, the most important length is the wake width [6], but that quantity is a kind of result, not control parameter.

3.2 Turbulent kinetic energy

Turbulent kinetic energy (TKE, K) is average kinetic energy associated with vortices and other coherent flow

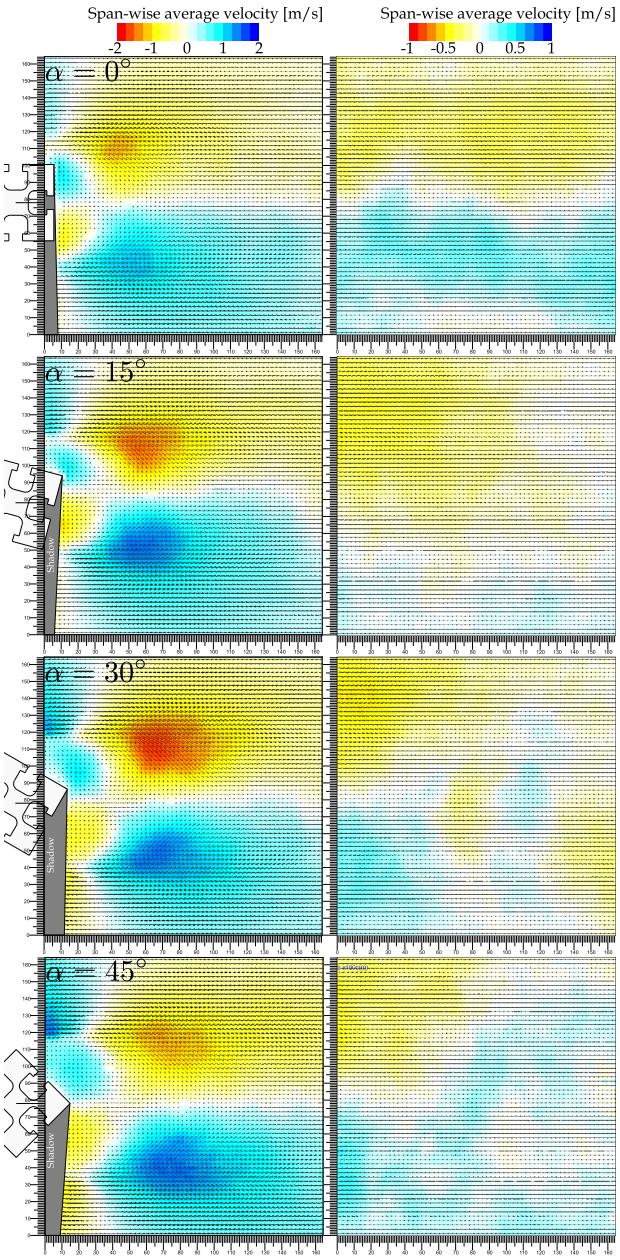

Fig. 2. Spatial distribution of the of the averaged span-wise velocity. Stream-wise velocity is 5.0 m/s, corresponding $Re = 1.5 \cdot 10^4$. The angle of attack α is from top 0°, 15°, 30° and 45° respectively. Note that the legend limits are different in left and right column.

structures, which the turbulence consists of. It is calculated as *variance* of velocity, i.e.

$$K(\vec{x}) = \frac{1}{2}\left(\left\langle u^2(\vec{x}) + v^2(\vec{x})\right\rangle_T - \langle u(\vec{x})\rangle_T^2 - \langle v(\vec{x})\rangle_T^2\right) \quad (1)$$

Where u and v denote the x- and y-component of the velocity vector, $\vec{x}$ is location and $\langle\cdot\rangle_T$ denote the averaging over time, i.e the ensemble averaging in this case of relatively „slow“ PIV.

The flow is naturally three-dimensional, while we have measured only the planar cut, therefore we lack any information about the third velocity component w.

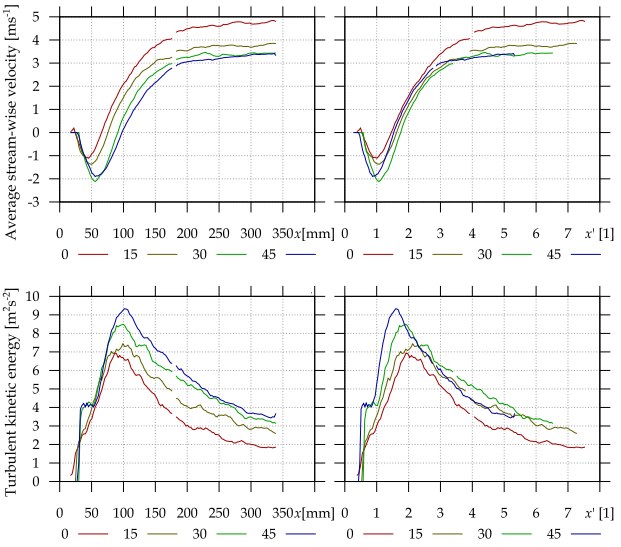

Fig. 3. Top: the development of of the average stream-wise velocity on the wake axis. The drop at $x = 180$ mm is caused by gluing the data from the two cameras. **Bottom**: the development of the turbulent kinetic energy along the wake axis. Color depicts the angle of attack: red for 0°, yellow for 15∘, green for 30° and blue for 45°. **Left**: the distance x is in [mm] counted from the axis of the obstacle. **Right**: the stream-wise distance x' is normalized by the crosssectional size of the obstacle, i.e. $x' = (x/a) \cdot \cos\alpha$, where $a = 45$ mm is the side of the studied aluminum profile.

Equation (1) can be rewritten by using the energies of instantaneous velocity field E and of averaged velocity field E_T as $K = E - E_T$, where $E = \frac{1}{2}\left\langle \vec{u}^2 \right\rangle_T$ and $E_T = \frac{1}{2}\langle\vec{u}\rangle_T^2$.

The turbulent kinetic energy is dominantly produced by the fluctuations of span-wise velocity v. The stream-wise one is dominant only in the narrow shear layer just on sides of the obstacle, while the fluctuations of the span-wise component v are massive in the wake axis, where the structure similar to „von-Kármán vortex street“ splits the direction of span-wise velocity. This effect is displayed in figure 5 for single angle of attack $\alpha = 15°$, but for other angles this behavior is similar. This behavior is observed in the wake past airfoil [7–9] and even in grid turbulence [10].

3.3 Distribution of span-wise velocity

The swapping direction of the span-wise velocity component in the wake can be visible from the instantaneous velocity fields and from the probability density function of this velocity component in the wake (both is displayed in figure 6).

Probability density function of span-wise velocity component v is plotted in figure 6 (b) and (c) as a function of non-dimensionalized span-wise velocity $v' = (v - \langle v\rangle)/\sigma[v]$, where the averaging $\langle\cdot\rangle$ and standard deviation $\sigma[\cdot]$ is performed in respect to the data points counted in the histogram. The double peak observable in the entire

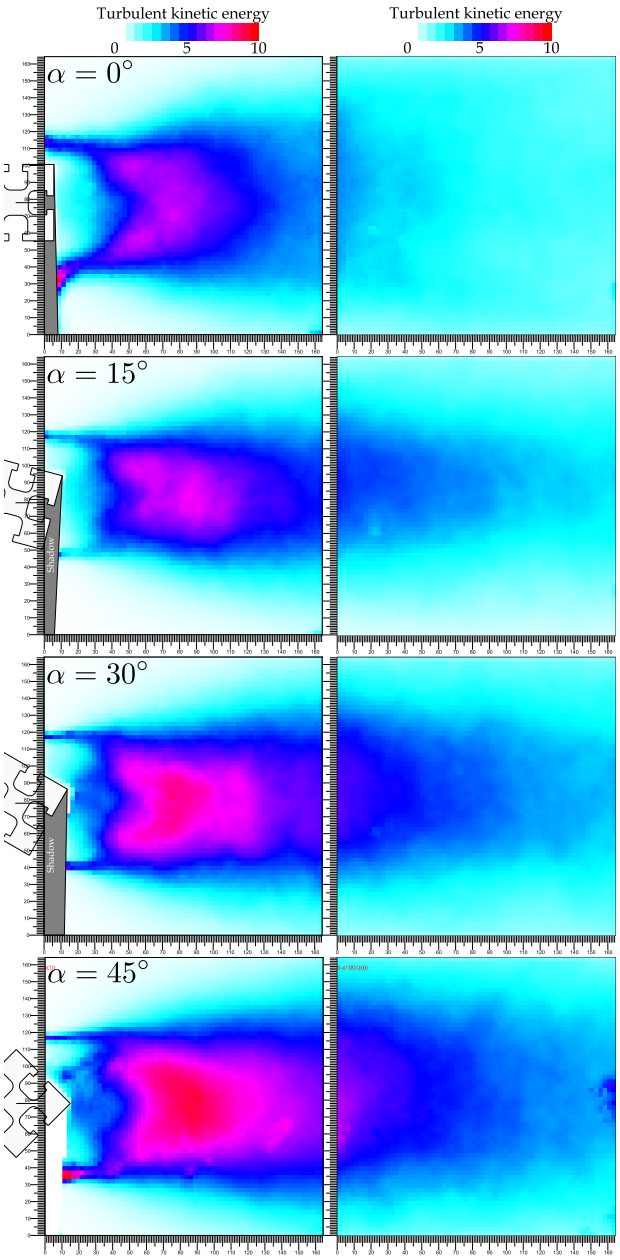

Fig. 4. Spatial distribution of the of the turbulent kinetic energy. Stream-wise velocity is 5.0 m/s, corresponding $Re = 1.5 \cdot 10^4$. The angle of attack α is from top 0°, 15°, 30° and 45° respectively. The data at 45° contain more noise due to measuring during the sunny days.

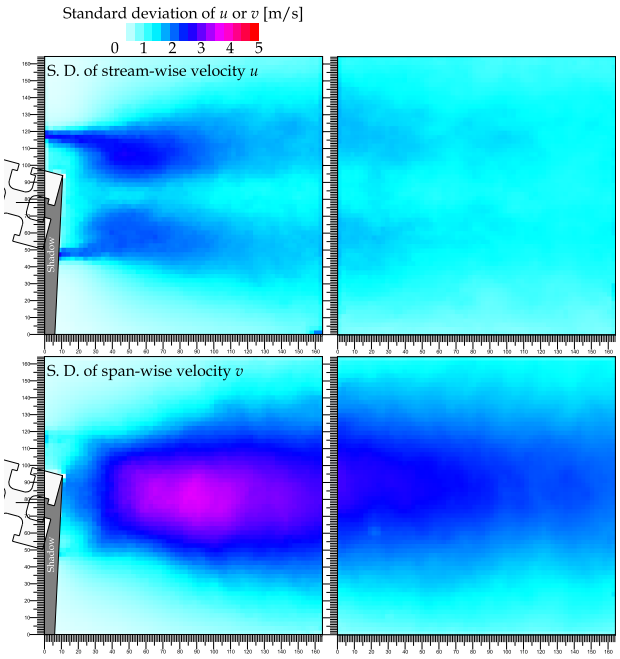

Fig. 5. Comparison of the standard deviations of stream-wise velocity u (**top**) and span-wise velocity v (**bottom**). Here are displayed only data at angle $\alpha = 15°$, other data have similar ratio of these two components.

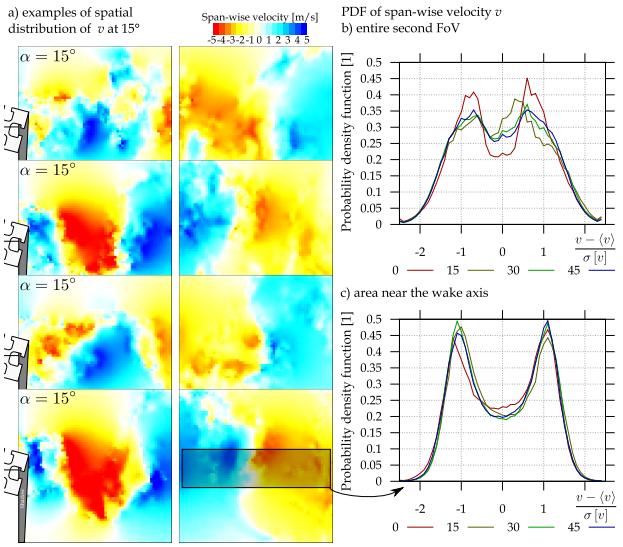

Fig. 6. Left: example of few instantaneous fields of span-wise velocity v at angle $\alpha = 15°$ and stream-wise velocity $u = 5$ m/s. **Right**: probability density functions of span-wise velocity in the entire second field of view (**b**) and in the limited area (**c**) near the wake axis. This area is depicted in the bottom image of the instantaneous velocity as a gray rectangle.

field of view clearly suggest the two dominant velocity directions. The fact, that this signal comes from the wake is even supported by selecting only that area for the processing, which is done in figure 6(c), and where a pair of symmetrical maxims is dominating the distribution.

Note that the maximum frequency of the PIV system is 7.4 Hz, which is very slow in comparison with the typical processes in the flow at the probed velocity (5 m/s), because during the time between the consecutive frame pairs (the frames are photographed in pairs delayed by few microseconds) the fluid moves by around 675 mm and thus it leaves not only the field of view, but also the tunnel test section. Therefore we cannot use the *slow* PIV data for determining the *Strouhal number* from the characteristic frequency of large vortices in the wake, as it is done e.g. in [11]

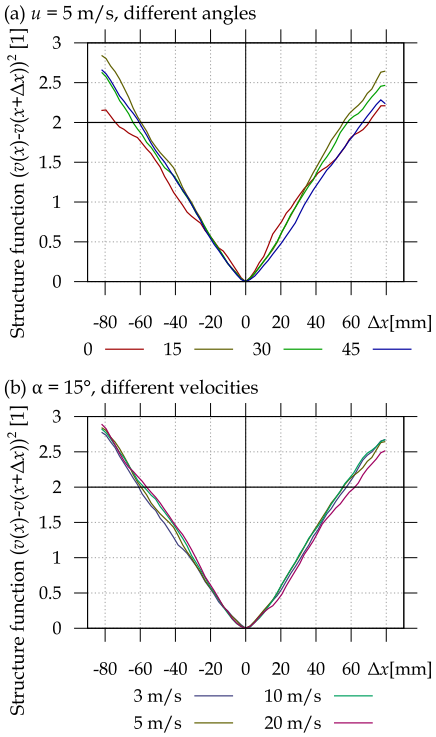

Fig. 7. Top: structure function S^2_{vv} of the span-wise velocity as a function of Δx, stream-wise velocity $u = 5\,\mathrm{m/s}$, different colors represent different angles of attack. **Bottom**: structure function S^2_{vv} for different velocities at constant angle of attack $\alpha = 15°$.

3.4 Structure function of span-wise velocity

The structure function [12] of second order of the span-wise velocity component v is defined as

$$S^2_{vv}(\vec{x}, \Delta\vec{x}) = \frac{\left\langle (v(\vec{x}) - v(\vec{x}+\Delta\vec{x}))^2 \right\rangle_T}{\sigma_T[v(\vec{x})] \cdot \sigma_T[v(\vec{x}+\Delta\vec{x})]} \qquad (2)$$

where $\vec{x}$ denote the reference point, which has been chosen at the wake axis in the center of the second field of view, i.e. 270 mm i.e. $6 \cdot a$ from the obstacle axis. $\Delta\vec{x}$ is the relative vector from the reference point $\vec{x}$ to the probed point, where the structure function is calculated. σ_T means the standard deviation in respect to time, i.e. ensemble in this case of relatively slow PIV. S^2_{vv} thus says, how much is the value of v at the point $\vec{x}$ statistically different from the value of v at point $\vec{x} + \Delta\vec{x}$. When the values are same (which is identically fulfilled when $\Delta\vec{x} = 0$), the value of $S^2 = 0$, when the values are *not correlated*, the value of $S^2 = 2$.

This function is autostructure function as it probes the same quantity only in different locations. There can be defined also a crossstructure function S_{uv}, which relates the span-wise and the stream-wise velocity component; we do not discuss it in this article.

As has been proven in [12], the S^2 is in close relation to the autocorrelation function C_{vv} as $S^2_{vv} = 2-2C_{vv}$, when the sample size is infinite. But, in respect to autocorrelation function, the structure function is not sensitive to the mean value and it converges better.

Figure 7 shows the structure function S^2_{vv} in respect to the stream-wise displacement Δx (without vector, just displacement along the wake axis). We can see, that in all cases S^2_{vv} reaches the value of 2 (where it is considered to be not correlated) straightly continuing even up. This observation suggests, that the values are in phase shift by 90° instead of not correlated, and, if we would have larger field of view, we could probably observe a maximum at double the distance of reaching 2 and then drop down and another minimum at 4× this distance. But this are just speculations not supported by measured data. But, what is clearly observable is, that the structure function of span-wise velocity does not depend on the imposed stream-wise velocity – it is surprisingly similar. On the other hand, it changes little bit with angle of attack, but not in a systematic way.

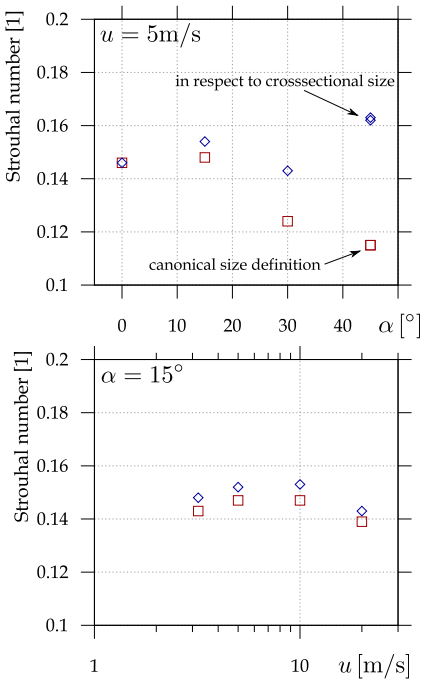

Fig. 8. Top: dependence of the Strouhal number Sr on the angle of attack α at constant imposed stream-wise velocity $u = 5\,\mathrm{m/s}$. **Bottom**: Strouhal number as a function of imposed stream-wise velocity u at constant angle of attack $\alpha = 15°$. Red squares represent the „standard“ definition with the obstacle size as the characteristic length-scale, while blue diamonds use the crosssectional size of the obstacle, i.e. $a' = a/\cos\alpha$, where $a = 45\,\mathrm{mm}$ is the side of the studied aluminum profile.

The distance, where the autostructure function reaches the value of 2, which we can consider to be one quarter of the spatial period of the „von-Kármán-like-structure“, is $R_+ = 58.5\,\mathrm{mm}$ and $R_- = 55.7\,\mathrm{mm}$, where the subscript + and − means the stream-wise direction or the counter-stream-wise one; it is not surprise that the range in the stream-wise direction is larger, as the convective average velocity grows along the wake axis. We can recalculate the spatial period to the time-period by using the stream-wise velocity in the wake axis and calculate the *Strouhal*

number Sr

$$\mathrm{Sr} = f\frac{L}{U} = \frac{u_{\mathrm{wake}}}{2\,(R_+ + R_-)} \cdot \frac{a}{u} \tag{3}$$

where u_{wake} is the convective stream-wise average velocity at the wake axis in the distance of the probed point, u is the imposed stream-wise velocity, a denotes the size of the aluminum profile side and R_+ and R_- are the just discussed distances, where autostructure function of span-wise velocity reaches the value 2, which is estimated to be in one quarter of the spatial period. Similarly to the discussion above, we can use a *crosssectional size* of the obstacle $a' = a/\cos\alpha$, where $a = 45$ mm is the side of the studied aluminum profile.

Figure 8 shows, that this estimation of Strouhal number reaches the classical values for cylinder of square crosssection only approximately, e.g. Dutta et al. [11] report the value around 0.14 with similar development with angle of attack – first an increase with maximum at 22.5° and then faster decrease in a such way, that $\mathrm{Sr}\,(\alpha = 30°) < \mathrm{Sr}\,(\alpha = 0°)$ and $\mathrm{Sr}\,(\alpha = 45°)$ is smallest. Chauhan et al. [13] report the value of 0.143 for $\alpha = 0°$.

4 Conclusion

By using Particle Image Velocimetry (PIV) technique we observed wake behind a aluminum construction profile of 45 mm side. We investigated the dependence of the wake on the angle of attack for four different angles $\alpha = 0°$, 15°, 30° and 45° at velocity 5 m/s corresponding to side-based Reynolds number $Re = 1.5 \cdot 10^4$.

We found that there is a pair of recirculation vortices in the averaged field of view. The average stream-wise velocity in the near wake region is negative and it returns towards the imposed value along the wake axis. We observed, that this return collapses better, when the distance is calculated in crosssectional sizes of obstacle. The turbulent kinetic energy profile creates a plateau just behind the obstacle for angles of attack 30° and 45° but not for 0° and 15°; we do not have theoretical explanation at this moment. We confirmed, that the turbulent kinetic energy is caused mainly by the fluctuations in span-wise velocity, which is caused by the periodic structure similar to the von Kármán vortex street in the wake of circular cylinders. Its existence causes the double peak shape of the probability density function (PDF) of the span-wise velocity in the wake area. The second order structure function grows almost linearly over the value of 2, which corresponds to not correlated values, but due to the periodic character we believe, that it means 90° phase shift rather than loss of correlation. Based on this assumption, we estimated the value of Strouhal number, which is a nondimensionalised frequency of a such pattern, and we approximately fit the values reported in literature for square cylinders.

In the future we plan to check our result based on artificial assumptions (i.e. that the value of structure function of 2 corresponds to one quarter of the spatial period, that the convective velocity is the velocity at the point probed by the structure function) by using Laser Doppler Anemometry technique (LDA), which is a method with very good time-resolution and thus it is suitable to, among others, direct measurement of Strouhal number.

Acknowledgements We thank to Ing. Buhumil Laštovka for valuable technical help. This work was supported by the project of Technology Agency of the Czech Republic TA ČR No TH02020057 „Program Epsilon“.

References

[1] V. Yanovych, D. Duda, V. Uruba, European Journal of Mechanics, B/Fluids **85**, 110 (2021)
[2] C. Tropea, A. Yarin, J.F. Foss, *Springer Handbook of Experimental Fluid Mechanics* (Springer, Heidelberg, DE, 2007)
[3] D. Jašíková, M. Kotek, R. Horálek, J. Horčička, V. Kopeckỳ, ILASS – Europe 2010, 23rd Annual Conference on Liquid Atomization and Spray Systems, Brno, Czech Republic, September 2010 **23** (2010)
[4] V. Koschatzky, P.D. Moore, J. Westerweel, F. Scarano, B.J. Boersma, Experiments in Fluids **50**, 863 (2011)
[5] M. Hirota, H. Fujita, H. Yokosawa, H. Nakai, H. Itoh, International Journal of Heat and Fluid Flow **18**, 170 (1997)
[6] D. Duda, V. Yanovych, V. Uruba, Energies **14**, 4712 (2021)
[7] D. Duda, V. Yanovych, V. Tsymbalyuk, V. Uruba, Energies **15**, 1227 (2022)
[8] I. Solís-Gallego, A. Meana-Femández, J.M.F. Femández Oro, K.M.A. Argüelles Díaz, S. Velarde-Suárez, Journal of Applied Fluid Mechanics **10**, 1013 (2017)
[9] V. Yanovych, D. Duda, V. Uruba, P. Antoš, SN Appl. Sci. **3**, 885 (2021)
[10] D. Duda, V. Yanovych, V. Uruba, Processes **8**, 1355 (2020)
[11] S. Dutta, P.K. Panigrahi, K. Muralidhar, Journal of Engineering Mechanics **134**, 788 (2008)
[12] E.O. Schulz-DuBois, I. Rehberg, Applied physics **24**, 323 (1981)
[13] M.K. Chauhan, S. Dutta, B.K. Gandhi, Journal of Wind Engineering and Industrial Aerodynamics **184**, 342 (2019)